Abdominal Radiology (2023) 48:91–105
https://doi.org/10.1007/s00261-021-03323-1

SPECIAL SECTION: BENIGN BILIARY DISEASE

Magnetic resonance cholangiopancreatography: pitfalls in interpretation

Malak Itani[1] · Neeraj Lalwani[2] · Mark A. Anderson[3] · Hina Arif-Tiwari[4] · Raj Mohan Paspulati[5] · Anup S. Shetty[1]

Received: 2 September 2021 / Revised: 13 October 2021 / Accepted: 15 October 2021 / Published online: 28 October 2021

Abstract

Magnetic resonance cholangiopancreatography (MRCP) has become a widely accepted noninvasive diagnostic tool in the assessment of pancreatic and biliary disease. MRCP essentially exploits extended T2 relaxation times of slow-moving fluid and delineates the outline of biliary and pancreatic ducts on T2-weighted images. In order to maximize the clinical implication of MRCP, it is of utmost importance for radiologists to optimize the acquisition technique, be aware of patient-related factors and physiologic changes than can affect its performance and interpretation. It is critical to understand the most common artifacts and pitfalls encountered during acquisition and interpretation of MRCP. We provide a general overview of the different pitfalls encountered in MRCP and pearls on how to manage them in real-world practice.

Graphic abstract

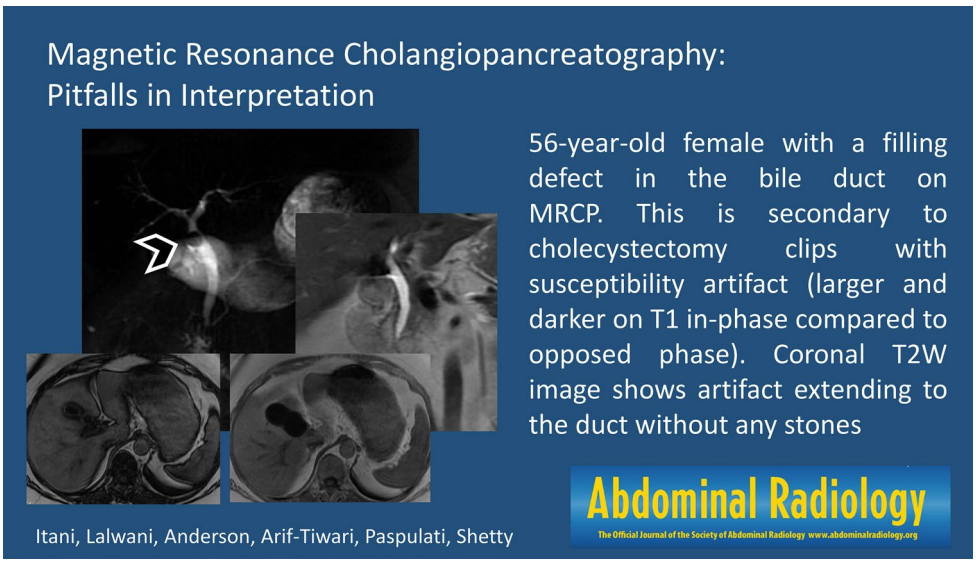

Keywords Magnetic resonance cholangiopancreatography · MRCP · Pitfalls · Artifacts

✉ Malak Itani
mitani@wustl.edu

[1] Mallinckrodt Institute of Radiology, Washington University in St. Louis, 510 S Kingshighway Blvd, St. Louis, MO 63110, USA

[2] Department of Radiology, Virginia Commonwealth University, Richmond, VA 23298, USA

[3] Department of Radiology, Massachusetts General Hospital, Boston, MA 02114, USA

[4] Department of Medical Imaging, University of Arizona, Tuscon, AZ 85724, USA

[5] Department of Radiology, University Hospital Cleveland Medical Center, Cleveland, OH 44106, USA

Introduction

Today, magnetic resonance imaging (MRI) plays an essential role in evaluating the biliary tract. Although ultrasound (US) and computed tomography (CT) were used before MRI for evaluating biliary pathology, MRI provides more comprehensive evaluation than ultrasound, and superior soft tissue contrast compared to CT, which enabled MRI to quickly become the gold standard non-invasive diagnostic imaging modality of choice. Magnetic resonance cholangiopancreatography (MRCP) was introduced in the late 1980s and early 1990s [1, 2]. MRCP relies on the long T2 relaxation time of fluid to image the biliary tree and pancreatic ducts with suppression of adjacent tissue signal. This characteristic provided an ideal means for a non-invasive, sensitive, and accurate detection of pancreaticobiliary ductal abnormalities.

With rapid technical improvements, there was a parallel increase in imaging indications as well as volume of studies. MRCP is now offered in most hospitals and outpatient imaging centers and is one of the commonly performed abdominal MRI examinations. The value of this study, however, depends on the diagnostic information that it can give, which is strongly tied to acquisition technique, image quality, and accurate interpretation.

The goal of this manuscript is to review the fundamentals and pitfalls of MRCP image acquisition and interpretation in order to enable radiologists to extract the most useful and clinically relevant interpretation within each specific clinical context (Table 1).

Technique

MRCP sequences are built upon a T2-weighted turbo spin echo acquisition. Lengthening the TE, on the order of several hundreds of milliseconds, results in capturing transverse magnetization of water, which has the longest T2, at a time when other tissues (liver, pancreas, fat, etc.) have little to no residual transverse magnetization due to T2 decay. MRCP is typically performed with fat suppression to further ensure that fat contributes no signal. The two families of MRCP acquisitions are 2D and 3D sequences (Table 2). Both types of acquisitions should be performed in a standard MRCP protocol with the goal of at least one of the sequences being diagnostic (Figs. 1 and 2).

2D sequences are performed as a breath-hold, single-slice, thick-slab coronal acquisition, typically 40–70 mm, positioned by the technologist to cover the pancreaticobiliary tree. The 2D sequence is modified from a single-shot half-Fourier turbo spin echo sequence (e.g., HASTE, Siemens Medical Solutions) to be heavily T2-weighted by lengthening the TR and TE. Multiple acquisitions can be performed sequentially in a radial fashion to obtain the entire

Table 1 Various artifacts on MRCP, causative factors, and ways to overcome them

Artifact	Cause	Solution
Discontinuity, duplication, stenosis, or dilation	Respiratory motion	For irregular breathing, get thick-slab 2D MRCP with breath hold. For regular/consistent breathing, get 3D MRCP. If both limited, consider compressed sensing MRCP
Dark bile on heavily weighted T2	Gadolinium (delayed phase of hepatobiliary contrast agent), blood, sludge, proteinaceous content	Correlation with clinical history, T2-weighted images, and in/opposed-phase images
Susceptibility	Pneumobilia or surgical clips	Correlate with axial T2, in/opposed-phase images, R2*, and other cross-sectional modalities
Flow artifacts	Dilated CBD or rapid change in caliber	Recognize central location of this artifact
Overlapping fluid	Ascites, duodenal or gastric fluid, thick slab overlying spinal canal	Paracentesis (ascites); fasting prior to MRCP or negative oral contrast (gastroduodenal fluid). Optimal orientation of thick-slab 2D MRCP (overlapping spinal canal)
Volume averaging underestimating or overestimating a stricture	MIP reconstruction	Always review source images and various reconstructions performed at different angles
Pseudocalculus sign	Contracted sphincter	Evaluate whether bile is surrounding the entire apparent defect or only its cranial aspect. Review other sequences as the contraction eventually resolves
Pulsation and vascular impressions	IVC, hepatic arterial branches, cavernous transformation	Recognize the smooth impression with no proximal dilation. Evaluate cause of apparent stenosis on post-contrast T1-weighted images

Table 2 Typical parameters for 2D and 3D MRCP

Technique	Comments	TR in ms	TE in ms	Slice thickness in mm	Field of view in mm	Matrix	Acquisition time
MRCP 2D Thick Slab T2 Single-Shot FSE	Breath hold	4500	750	70	300×300	384×384	5 s
MRCP 3D Volumetric T2 3D TSE CS-Respiratory Navigated	Free breathing	6000	700	1	285×380	576×768	90 s
MRCP 3D Volumetric T2 3D TSE CS-Breath Hold	Breath hold	2000	700	1	285×380	576×768	18 s
T2 Single-Shot FSE Coronal	Full abdomen coverage; multi-breath hold	1000	100	6	400×400	320×320	120 s
T1 3D Spoiled GRE Dixon	Acquire in phase and opposed phase, reconstruct fat-only and water-only; breath hold	6.68	2.39	3	308×380	260×320	14 s
T1 3D Spoiled GRE Dixon Multi-Echo	Acquire 6 progressively longer echoes, reconstruct fat-fraction and R2* maps; breath hold	15.6	2.38	3.5	304×380	256×320	18 s
T2 Single-Shot FSE Axial	Cover entire liver and pancreas; multi-breath hold	1000	100	4	308×380	260×320	150 s
T2 Single-Shot FSE Coronal	Cover central bile ducts and pancreas; multi-breath hold	1000	100	4	375×375	320×320	150 s
T2 Single-Shot FSE Sagittal	Cover common bile duct; multi-breath hold	1000	100	4	308×380	320×260	90 s
T1 3D Spoiled GRE Coronal Precontrast	Breath hold	3.47	1.27	3	400×400	320×320	14 s
T1 3D Spoiled GRE Axial Precontrast	Breath hold	4.12	2	3	308×380	260×320	12 s
If with contrast, add T1 3D Spoiled GRE Axial Arterial, Venous, Equilibrium, and 5 min delay	Breath hold	4.12	2	3	308×380	260×320	12 s each
If with contrast, add T1 3D Spoiled GRE Coronal Equilibrium	Breath hold	3.47	1.27	3	400×400	320×320	14 s

TR repetition time, *TE* echo time

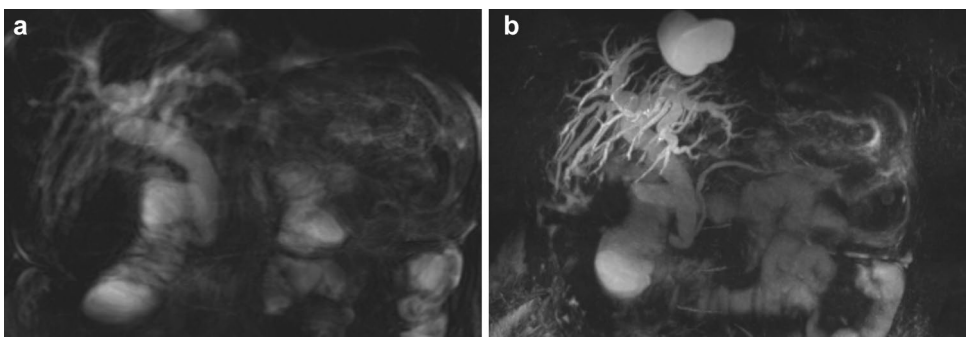

Fig. 1 Utility of acquiring 2D and 3D MRCP sequences: **A** Breath-hold 2D MRCP is degraded by motion artifact, as were other breath-hold sequences in this MRI. **B** Free-breathing 3D MRCP provides sharp depiction of the pancreaticobiliary tree, indicating that this patient, while unable to adequately hold their breath, was able to breathe consistently during the free-breathing acquisition

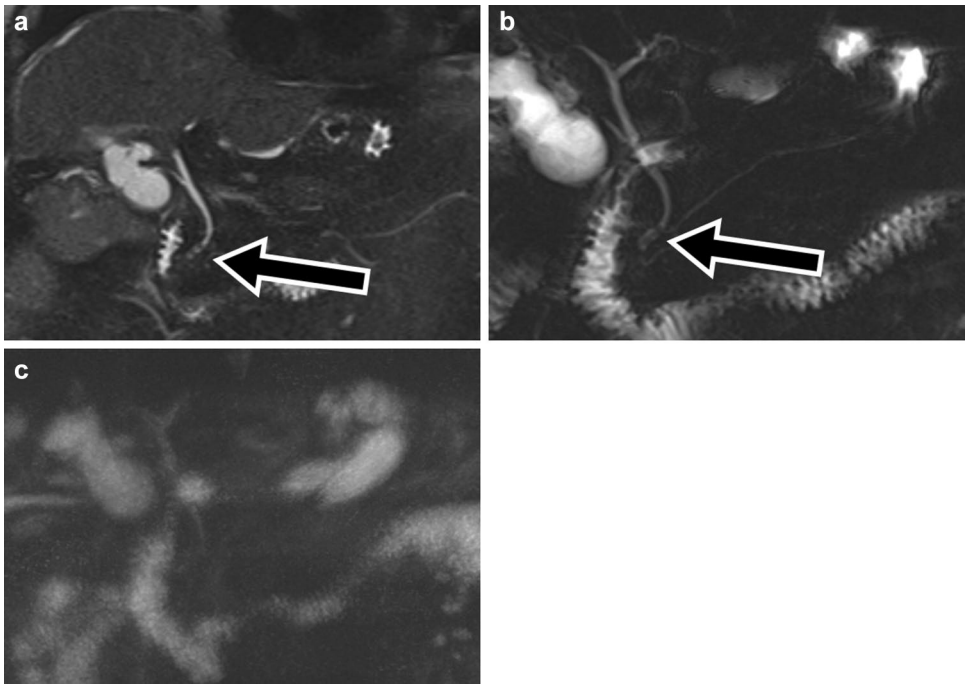

Fig. 2 Utility of acquiring 2D and 3D MRCP sequences: **A** Thin-slice coronal T2 HASTE shows distal choledocholithiasis (arrow), confirmed at ERCP. **B** 2D MRCP far better depicts the intraductal filling defects (arrow) than free-breathing 3D MRCP (**C**), likely due to inconsistent breathing resulting in motion blur

360° in 10–12 image slabs, although in practice a straight coronal and 30° obliques provide similar value in profiling the pancreatic duct and extrahepatic bile duct (Fig. 3). 2D sequences can be rapidly obtained and require no further postprocessing for image review, but because of their planar nature cannot be further manipulated. Images may also be degraded in patients with limited breath-holding capability.

3D sequences obtain a volumetric acquisition of the pancreatobiliary tree through a stack of thin slices. Due to the length of the 3D acquisition, which is typically 4–6 min, respiratory-navigation is typically used, in which the patient freely breathes during the acquisition and images are only acquired at end-inspiration or end-expiration with the diaphragm within a specified range. With more consistent

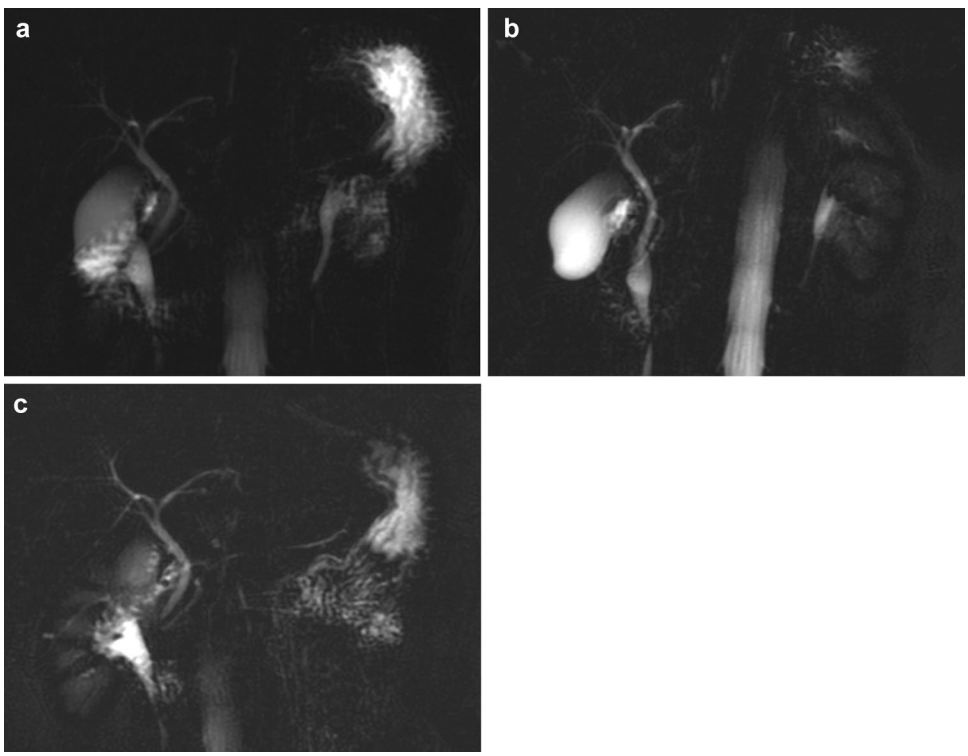

Fig. 3 Comparison of straight coronal and 30-degree thick-slab acquisitions: **A** 2D thick-slab MRCP coronal, **B** 30° clockwise oblique, and **C** 30° counterclockwise oblique acquisitions profile the bile duct and pancreatic duct well with only three acquisitions. Note that other fluid-filled structures (the stomach, spinal canal, and renal collecting systems) are also visible

breathing by the patient, the sequence is completed more rapidly and images are of higher sharpness with less motion artifact. After a volumetric data set is obtained, a maximum intensity projection (MIP) can be created, simulating the appearance of the 2D thick-slab MRCP. A rotating projection of the MIP can also be created, providing the ability to more optimally profile a region of interest, typically rotating in the coronal and craniocaudal planes. Finally, the source data can be reformatted in multiple planes, facilitating further investigation of the pancreaticobiliary tree that is not possible with 2D thick-slab MRCP. 3D MRCP should provide higher signal to noise ratio (SNR) and the ability to delineate subtle ductal abnormalities or anatomic variants in the patient who can breathe consistently (Fig. 4).

The time-to-echo remains critical during MRCP. A higher time-to-echo ensures that high intensity structures are highlighted and the background is suppressed. However, in addition to time-to-echo, T2 relaxation time of the fluid also determines the signal intensity on highly T2-weighted images. While normal bile is hyperintense, in the presence of hemorrhage, sludge, and/or high proteinaceous content like inspissated bile, the biliary structures may become invisible on MRCP. A similar phenomenon may be seen with inflammatory phlegmons and pseudocysts in pancreatitis.

Dual- and/or multi-echo T1 gradient echo sequences (used for chemical shift imaging and quantitative liver MRI, respectively) are not technically considered "MRCP" sequences but are invaluable for problem solving and should be part of a standard MRCP protocol. Dual echo sequences facilitate the detection of pneumobilia or metal as a source of susceptibility, as will be discussed below. An R2* sequence, if generated from processing of a multi-echo acquisition as part of quantitative liver MRI primarily for assessment of hepatic iron concentration, can also be used to assess for pneumobilia as a source of intrahepatic R2* hyperintensity (Fig. 5).

Technical pitfalls

Since fluid in the stomach and duodenum can obscure the ducts, patients are generally advised to fast for at least 2 h prior to the study. If gallbladder evaluation is also desired, then fasting should preferably be for 6–8 h. Negative oral contrast, such as pineapple juice, blueberry juice, or gadolinium-doped water, which results in T2 shortening of fluid in the gastrointestinal tract (due to high content of metals like manganese), may be used but is not necessary. If a patient is tachypneic, then placing them on oxygen before the MRI may help to achieve longer breath holds and provide consistent breathing for respiratory gating.

Spatial coverage should include at least the central intrahepatic and extrahepatic bile ducts and the pancreatic duct. For patients with cholangitis, the entire liver should be included, as cropped images can result in missing important information (Fig. 6). Excessive slab thickness or positioning of the slab too far posteriorly can result in obscuration of the pancreatic duct by cerebrospinal fluid in the spinal canal.

The need for gadolinium contrast administration with MRCP depends on the indication. In select scenarios, contrast might not be needed, including follow-up of pancreatic cystic lesions, and evaluation of choledocholithiasis [3]. For standard extracellular contrast agents, MRCP acquisitions can be performed prior to or after contrast administration, as gadolinium will not affect depiction of the bile ducts on heavily T2-weighted MRCP. However, if a hepatobiliary contrast agent such as gadoxetate disodium is used, MRCP should be performed either before contrast administration or soon after injection, as concentrated gadolinium in the bile ducts will shorten T2 relaxation time and may result in suboptimal visualization of the bile ducts (Fig. 7).

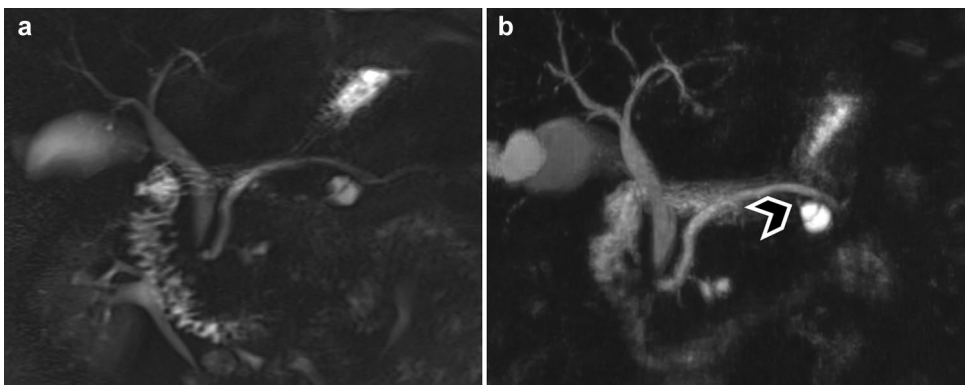

Fig. 4 Comparison of 2D and 3D MRCP: **A** 2D MRCP images show a cystic lesion in the distal pancreatic body with an internal septation. **B** 3D MRCP shows a tiny sidebranch (arrowhead) connecting the main pancreatic duct to a septated pancreatic cyst, confirming that this represents a branch duct intraductal papillary mucinous neoplasm

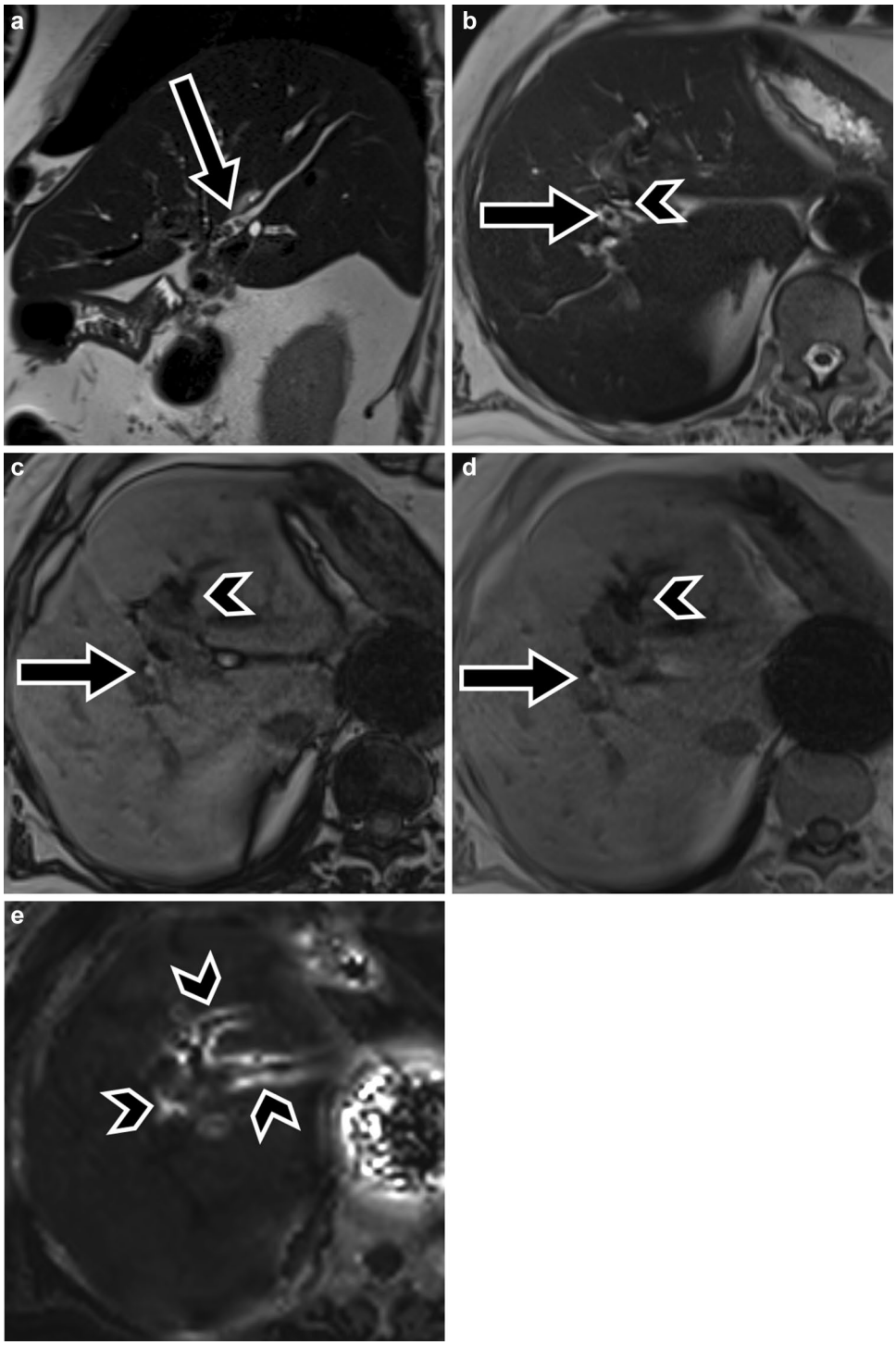

Fig. 5 MRCP for differentiating pneumobilia from stones: 73-year-old man with recent cholangitis managed with biliary stent. **A** Coronal and **B** axial T2-weighted images demonstrate hepaticolithiasis in the right hepatic duct (arrows) and pneumobilia (arrowheads) on the same axial slice. Compared to **C** opposed-phase images, pneumobilia blooms on **D** longer TE in-phase images and is readily identified as linear hyperintensity on **E** R2* maps automatically generated as part of quantitative liver MRI (Siemens LiverLab)

Artifacts

Motion artifacts, commonly from respiration, can cause apparent discontinuity, duplication, stenosis, or dilation of the biliary or pancreatic ducts (Fig. 8) [4]. This emphasizes the importance of reviewing the original thin-slice images. Additionally, volume averaging on thick slab and MIP images can obscure small filling defects or can cause overestimation or underestimation of a stricture [5]. Therefore, MIP images should always be interpreted with source images and reconstruction should be performed at different angles to differentiate an actual lesion from a pseudolesion.

Periampullary lesions or terminal duct choledocholithiasis require special attention. Sometimes, the contraction of the distal sphincter of the common duct can imitate an impacted choledocholithiasis or stricture (pseudocalculus

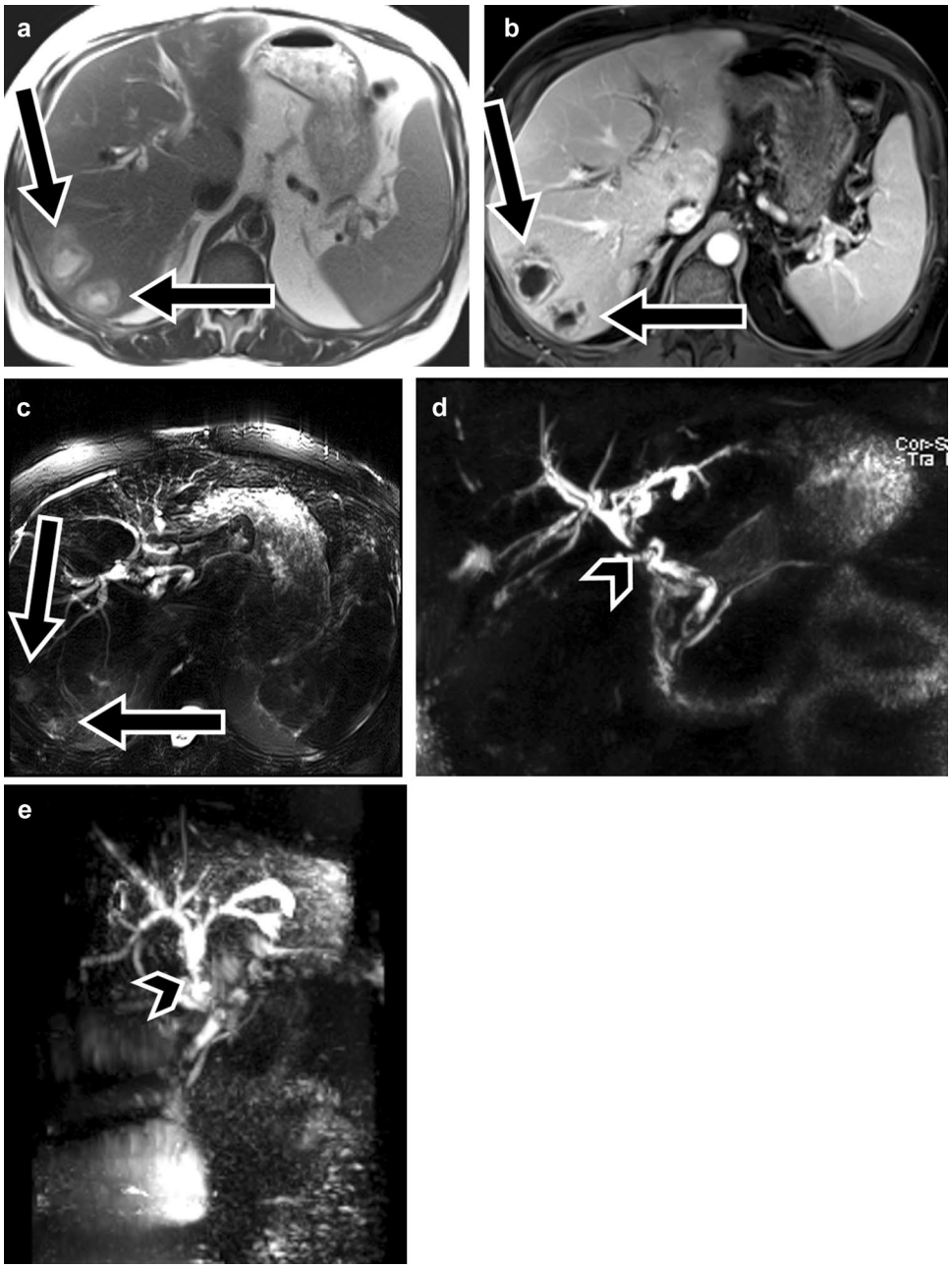

Fig. 6 Importance of the entire liver on MRCP: **A** Axial T2-weighted, **B** post-contrast T1-weighted fat saturated in the portal venous phase, and **C** axial heavily T2-weighted/MRCP source images demonstrate hepatic abscesses post-orthotopic liver transplant (arrows). There is a post-anastomotic stenosis in the common bile duct (arrowheads) better appreciated on **D**, **E** MRCP images. The peripheral abscesses can be missed if the MRCP images are cropped to include only the central ducts; they can also be missed on **E** rotated MRCP images

sign). A real stone is usually encircled with hyperintense bile. If only the upper margin of the defect is outlined with bile, a pseudolesion must be considered. The contracting sphincter is a transient finding and can disappear during a repeated acquisition. Additionally, reconstructing MIP images at different angles can help differentiate a pseudolesion from an actual lesion. A pseudolesion will disappear, while a real lesion will persist on all sequences and reconstructions (Fig. 9).

On the newest generation of MR scanners, compressed sensing (CS) MRCP can be utilized to markedly reduce acquisition time of 3D MRCP with undersampling of k-space, data transformation into a sparse projection, and non-linear optimized iterative reconstruction to reconstruct images with acceptable quality. CS reduces the typical acquisition length of a free-breathing 3D MRCP two to three times (1.5 to 2 min vs 4–6 min) [6]. CS can also be used to perform a breath-hold 3D MRCP, dramatically reducing acquisition time from minutes to seconds. The reduction of time allows for performing both free-breathing and breath-hold CS MRCP in approximately half the time than standard free-breathing 3D MRCP, improving the likelihood of diagnostic 3D MRCP in patients who breathe irregularly and patients who cannot hold their breath (Fig. 10) [7].

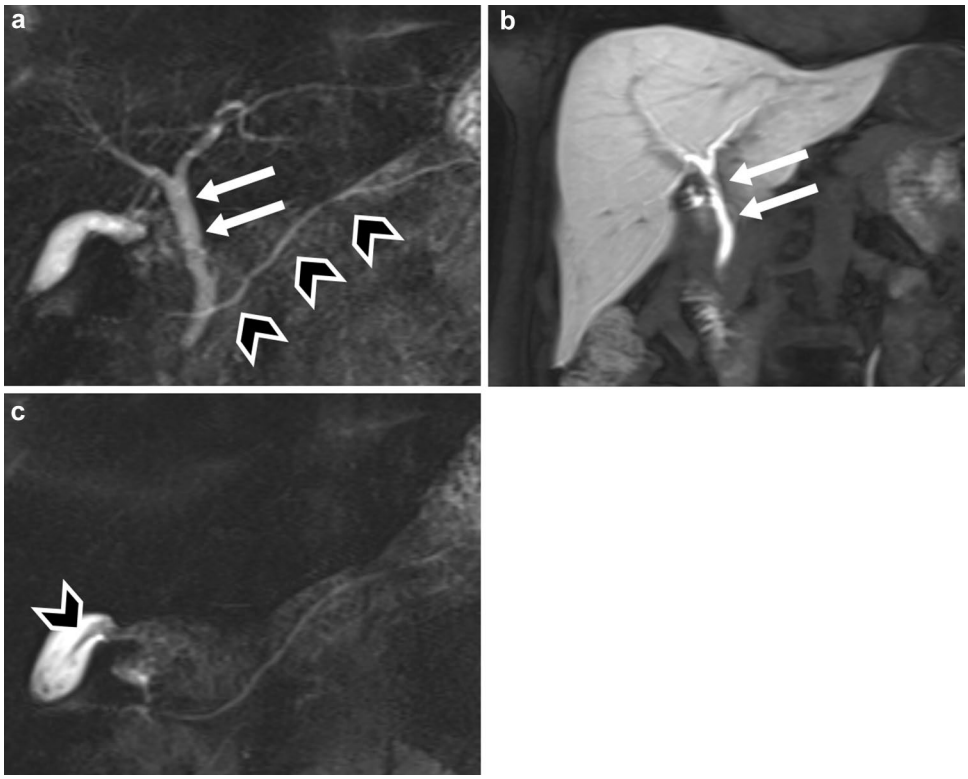

Fig. 7 T2 shortening on MRCP due to hepatobiliary contrast: MRCP in a 51-year-old female with metastatic breast cancer. **A** MRCP prior to contrast administration demonstrates normal biliary (arrows) and pancreatic (arrowheads) ducts. **B** Coronal T1-weighted fat-saturated image demonstrates hyperintense signal due to hepatobiliary contrast in the bile ducts (arrows). **C** MRCP images acquired after **B** show non-visualization of the bile ducts; this is secondary to gadolinium excretion causing shortening of T2 time and thus dark signal intensity of the bile ducts on T2-weighted MRCP images. Central linear hypointensity near the gallbladder neck corresponds to concentrated gadolinium entering the gallbladder (arrowhead)

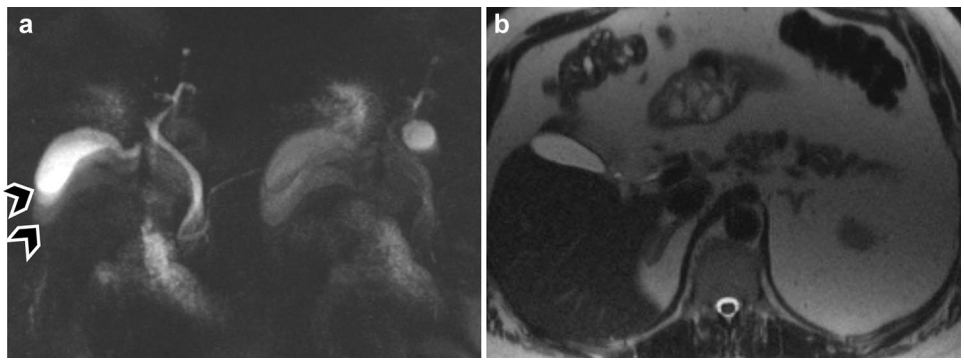

Fig. 8 Motion artifact on MRCP resulting in apparent gallbladder duplication: **A** 3D MRCP with motion artifacts resulting in apparent two gallbladders (arrowheads). **B** Axial T2 HASTE image demonstrates a single normal gallbladder

Susceptibility from adjacent metallic clips after cholecystectomy or other surgeries can result in apparent filling defects or strictures in the biliary tree. Pneumobilia can also be mistaken for a ductal stone, and the presence of diffuse pneumobilia may lead to a totally invisible duct on MRCP images. Correlation with axial T2-weighted images may shed light on the findings. Additionally, these issues can be clarified by reviewing T1-weighted in-phase and opposed-phase gradient echo images; if the filling defect is more pronounced in the longer echo in-phase image, then it is metal or gas rather than a stone (Fig. 11) [8]. The more recent usage of non-magnetic titanium clips for cholecystectomy has helped in reducing these artifacts [5]. Flow artifacts from bile motion are another potential filling defect; it is typically seen as a linear defect positioned centrally on axial images, as compared to biliary stones which are dependent, and gas which is non-dependent [9] (Figs. 12 and 13). Flow artifacts are more likely to be encountered when the CBD is dilated, at the point of insertion of a large cystic duct, and when the duct diameter changes over its length (change of over 4 times in caliber, e.g., from 8 to 2 mm) [5, 10, 11]. Flow artifacts occur only when the flow is orthogonal to the imaging plane, so the effect on the CBD is seen on the axial images and should not be present on coronal HASTE sequences. Pulsation artifacts from the inferior vena cava is an uncommon cause of apparent filling defects in the bile ducts on axial single-shot turbo spin echo sequences; pulsation is not seen on turbo spin echo images and this can be the problem solving sequence in differentiating this finding from a true filling defect [12].

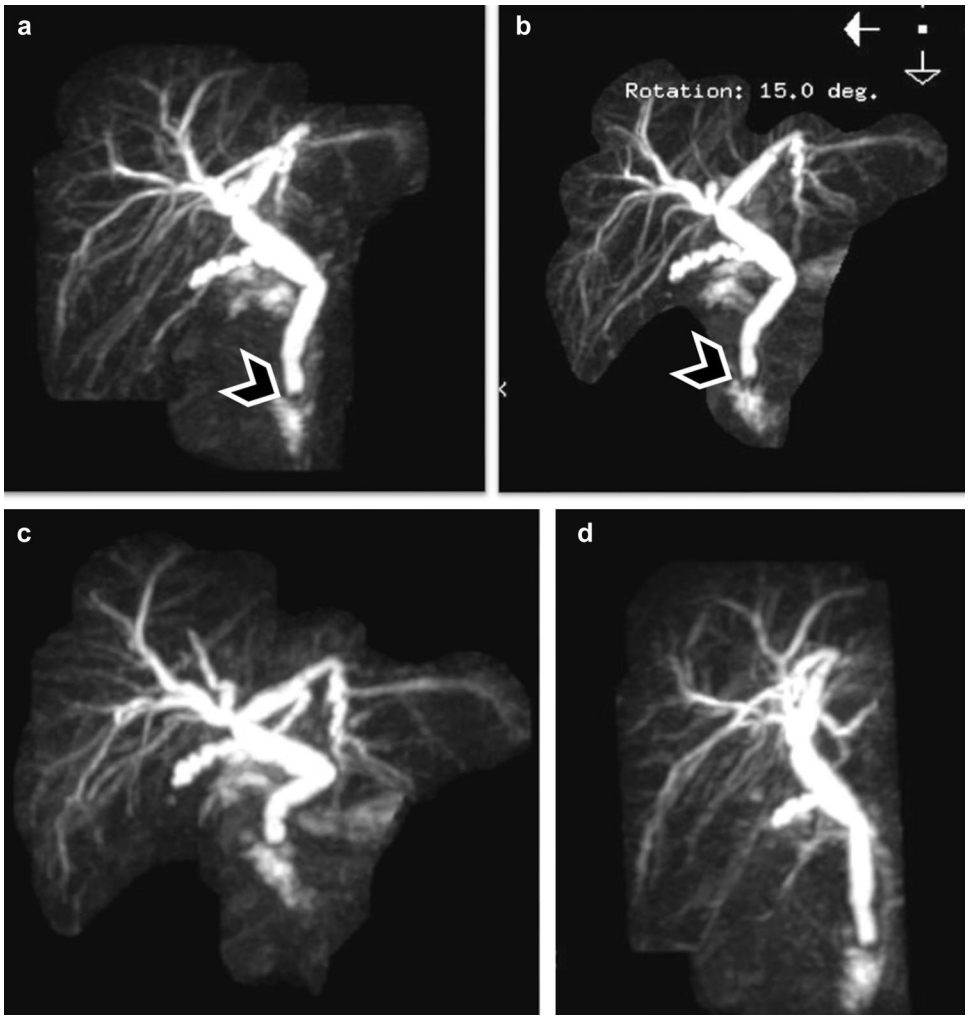

Fig. 9 Pseudocalculus sign due to sphincter contraction: **A** Coronal and **B** 15 degree rotated MRCP images demonstrate a filling defect in the distal common bile duct (arrowheads). Note that bile only outlines the superior margin of the defect. **C**, **D** Repeat MRCP images taken from different angles demonstrate resolution of the filling defect. This was a pseudocalculus secondary to spasm of the distal CBD sphincter

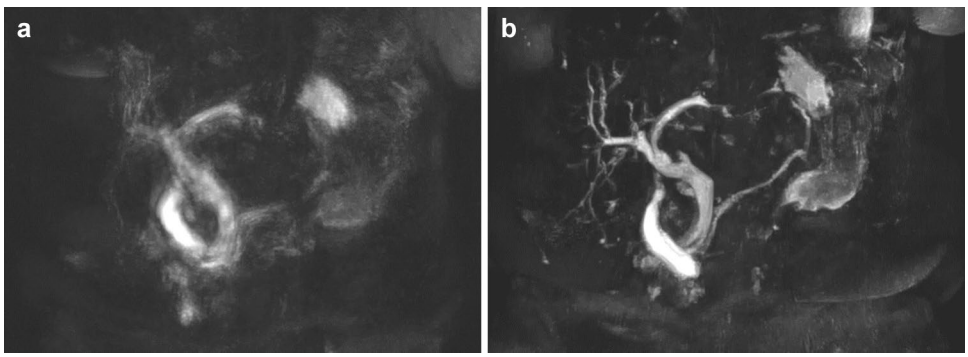

Fig. 10 MRCP in a patient with inconsistent breathing: **A** Free-breathing compressed sensing MRCP is degraded by motion artifact from irregular breathing during acquisition. **B** Breath-hold compressed sensing MRCP (right) provides much sharper delineation of the pancreaticobiliary tree, as the patient is able to hold their breath for the 18 s acquisition

Physiologic changes/normal variants

A variety of physiologic findings and variants can result in apparent strictures or other abnormalities of the biliary tree. Vascular impressions are most commonly caused by the right hepatic artery resulting in a pseudo-stricture of the common hepatic duct [13] and appear as a band-like area of narrowing with no proximal dilation [5]. Vascular impression can be caused by a variety of other vessels, including the cystic artery, proper hepatic artery and its branches, gastroduodenal artery, and collateral vessels namely in the setting of chronic portal thrombosis and cavernous transformation (Figs. 14 and 15); these vessels can cause apparent narrowing of different ducts, including the proximal CBD, the left or right hepatic ducts [13].

Stationary fluid in structures adjacent to the CBD can result in interpretation problems due to overlap of structures,

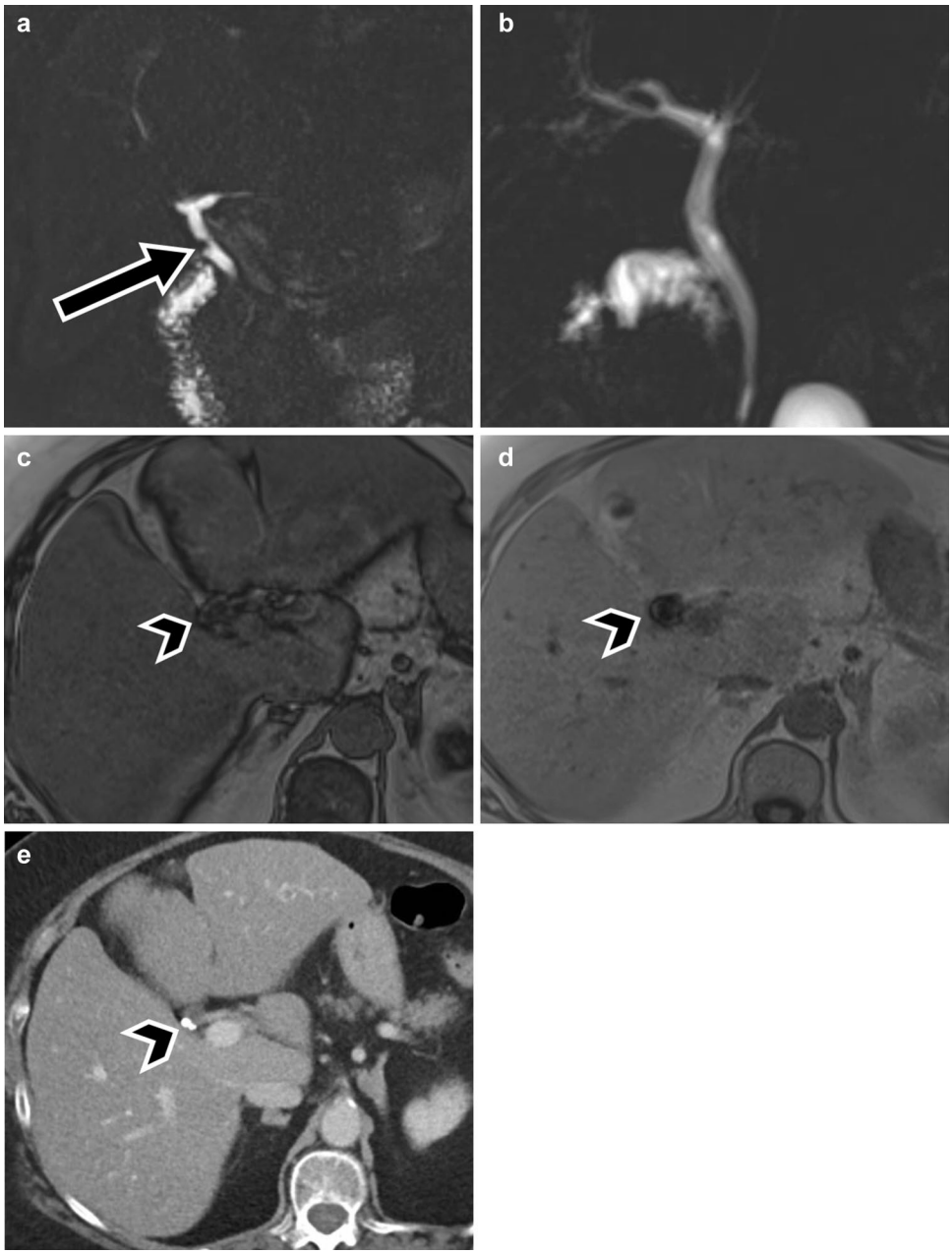

Fig. 11 Apparent filling defect on MRCP due to susceptibility artifact: **A** Coronal MRCP image in 72-year-old woman with abdominal pain shows an apparent focal stricture of the common hepatic duct on MRCP source images (arrow) with no abnormal upstream biliary dilation on **B** coronal MRCP maximum intensity projection (MIP) reconstruction. **C** Axial T1-weighted opposed-phase and **D** in-phase gradient echo images show that the filling defects result from a hypointense round structure (arrowhead) that appears larger, and darker, on in-phase images consistent with susceptibility artifact. This corresponded to cholecystectomy clips as demonstrated on (**E**) axial post-contrast CT

e.g., from ascites, fluid-filled bowel, or cystic collections. Evaluation of source data or rotating MIP may aid in viewing the duct without obscuration (Figs. 16 and 17). Fluid within a duodenal diverticulum may be mistaken for a cystic lesion, so evaluating for change in the lesion size or appearance on various sequences, as well as correlation with prior imaging studies, can be helpful in this situation.

The site of insertion of the cystic duct may appear as a filling defect in the bile duct when visualized en-face [5]. A long cystic duct that runs parallel to the CBD may give the false impression of a dilated CBD [5]. Also related to the cystic duct are flow artifacts that can be seen at the site of insertion of a large cystic duct [5]. Tortuosity of the pancreatic duct can mimic a dilated pancreatic sidebranch (Fig. 18).

In fasting patients, segmental collapse in the main pancreatic duct may be mistaken for a stricture, but the use of secretin can overcome this shortcoming as it increases the exocrine pancreatic secretions [4]. It is important to keep in mind that in addition to stones, true filling defects can be caused by tumor, blood, debris, and occasionally parasites or foreign objects [14, 15].

Fig. 12 Flow artifact on MRCP: Contrary to pneumobilia which is antidependent, and stones which are dependent, flow artifact is seen centrally within the bile duct (arrowhead)

Conclusion

In conclusion, a variety of artifacts, normal variants, and physiologic processes can result in pseudolesions and apparent pathology on MRCP. The radiologist has to be aware of these pitfalls and know how to overcome them with proper patient preparation, optimal imaging protocol, and familiarity with these findings as well as utilizing different sequences for optimal interpretation.

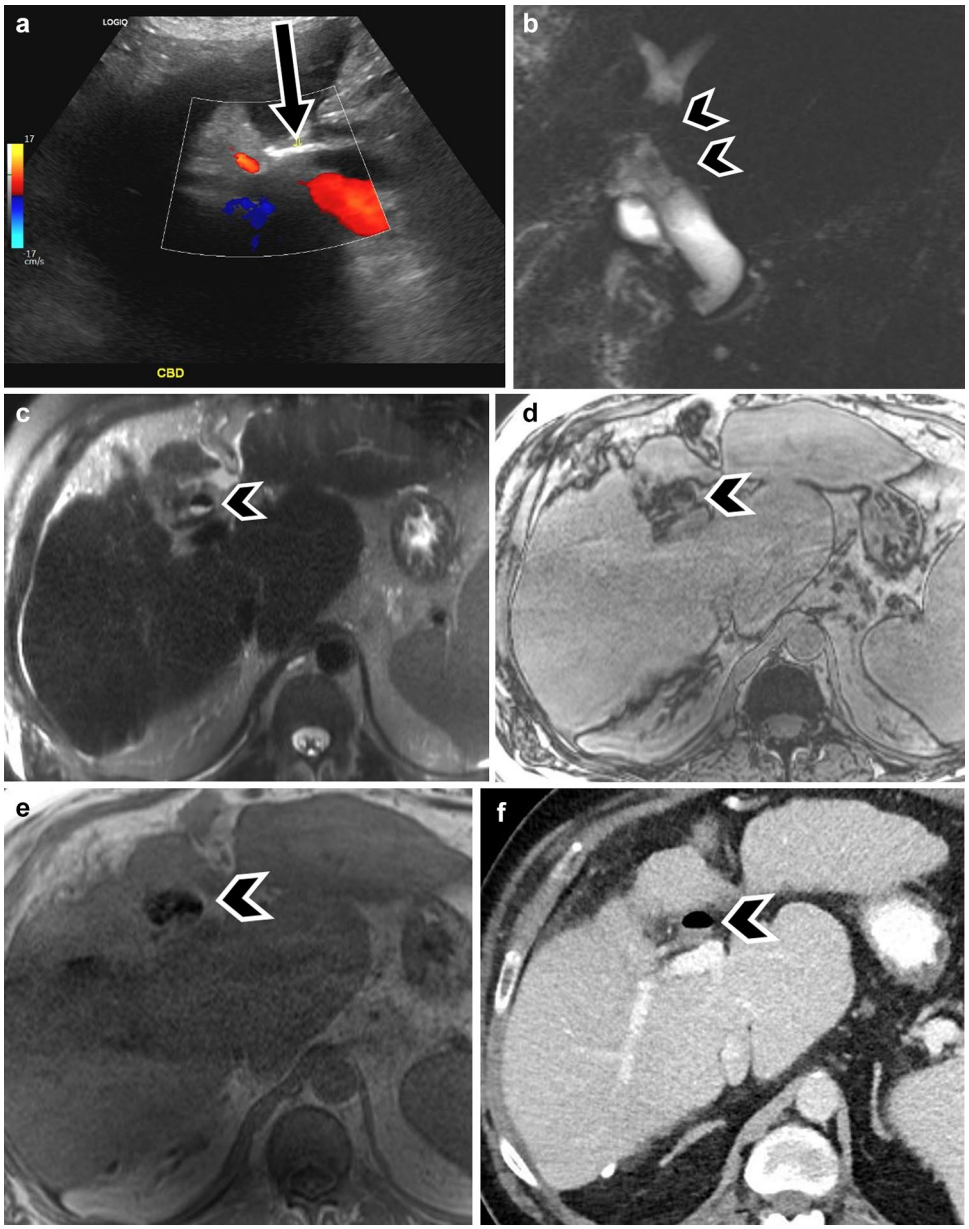

Fig. 13 Differentiating pneumobilia from stones on MRCP: 47 year-old man with recent cholecystectomy and prior ERCP presents with right upper quadrant pain. **A** Ultrasound performed at an outside facility showed an echogenic filling defect in the extrahepatic bile duct (arrow). **B** MRCP thick-slab coronal image confirms the filling defect (arrowhead). (C) Axial T2-weighted images show that the filling defect is in the anterior portion of the duct, consistent with an anti-dependent position, typical of gas, rather than stone (arrowhead). **D** Opposed-phase and **E** in-phase axial T1-weighted images demonstrate susceptibility artifact, typically seen with gas and metals. **F** CT confirms that this is consistent with pneumobilia and not a stone

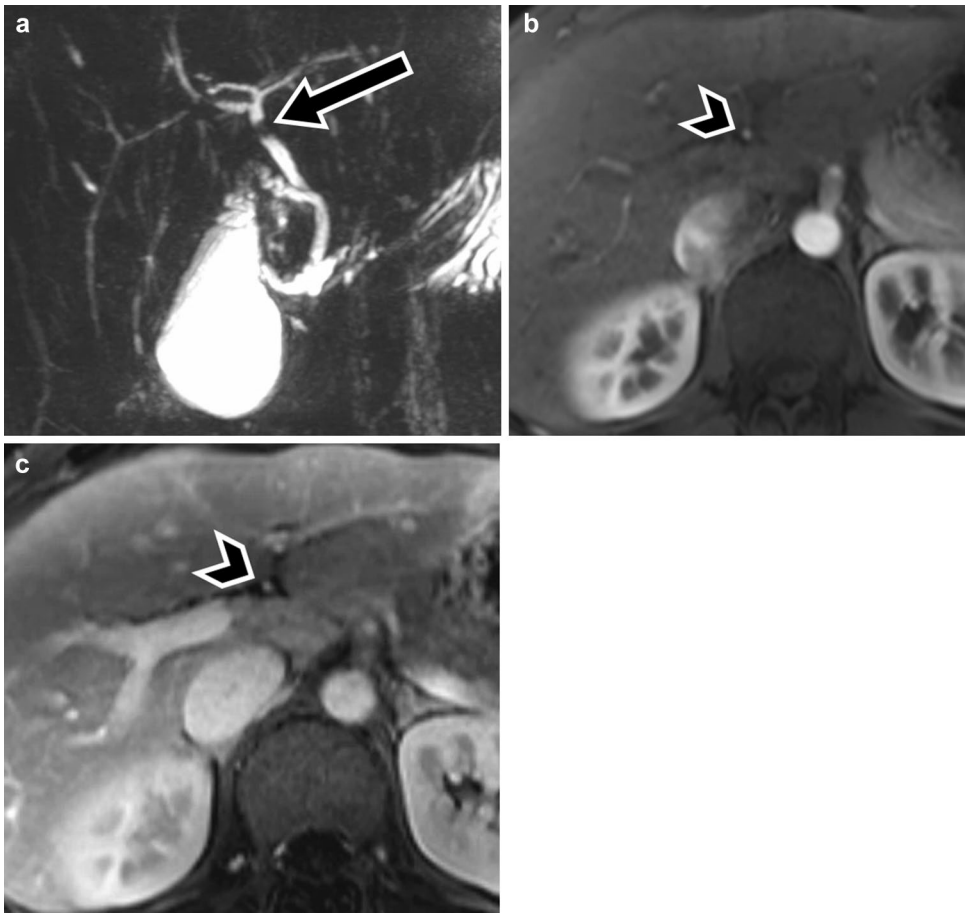

Fig. 14 Apparent filling defect on MRCP due to vascular impression: 22-year-old man with mildly elevated liver function tests. **A** Coronal MRCP maximum intensity projection (MIP) reconstruction, **B** axial T1-weighted arterial phase post-contrast MR image with fat saturation, and (C) axial T1-weighted portal venous phase post-contrast MR image with fat saturation show smooth impression or waist-like narrowing of the common hepatic duct (arrow in **A**) but no abnormal upstream bile duct dilation. Axial post-contrast images show the area of apparent narrowing on MRCP image to be at the site of the crossing proper hepatic artery (arrowheads in **B** and **C**). Findings are consistent with pseudostricture of the common hepatic duct due to vascular impression

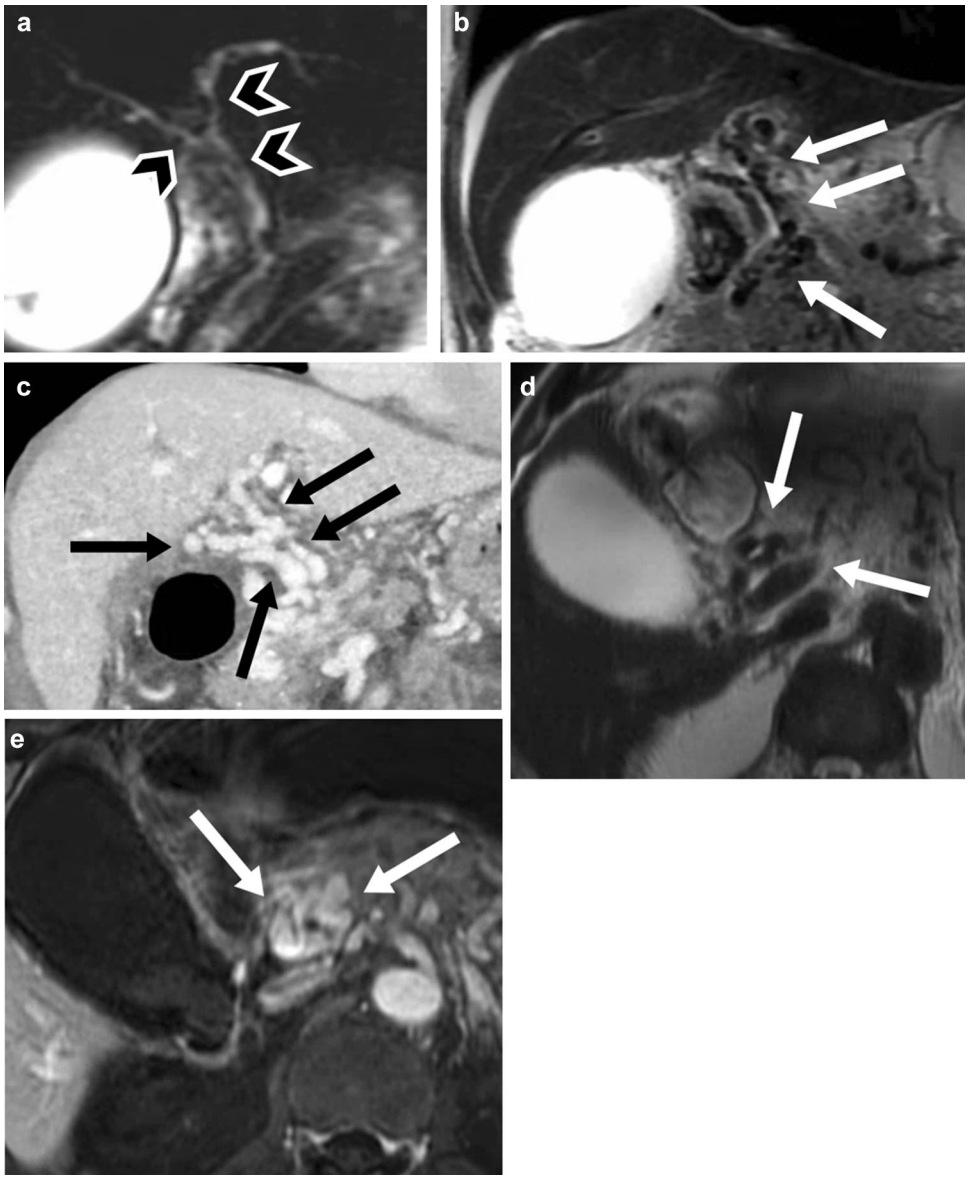

Fig. 15 Apparent filling defect on MRCP due to cavernous transformation: 77-year-old man with newly diagnosed pancreatic ductal adenocarcinoma of the pancreatic body causing portal vein occlusion with normal liver function tests. **A** Coronal MRCP maximum intensity projection (MIP) reconstruction, **B** coronal T2-weighted SSFSE image, **C** coronal contrast-enhanced CT, **D** axial T2-weighted SSFSE, and **E** axial portal venous phase post-contrast T1-weighted image with fat saturation through the central bile ducts show apparent beading and multifocal stricturing of the right and left hepatic ducts and extrahepatic bile duct without upstream dilation on MRCP image (arrowheads). T2-weighted and post-contrast images show sequelae of cavernous transformation of the portal vein with multiple large peribiliary collaterals (arrows) causing external contour deformity of bile ducts simulating multifocal strictures

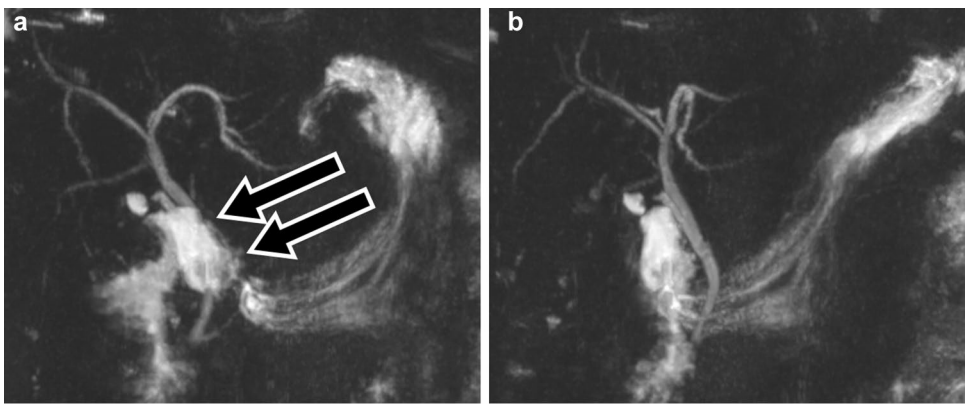

Fig. 16 Suboptimal MRCP due to duodenal fluid: **A** Straight coronal 3D MRCP MIP shows obscuration of the mid common bile duct by fluid in the duodenal bulb (arrows). **B** Rotation of the image on a rotating MIP series provides an unobstructed view of the common bile duct

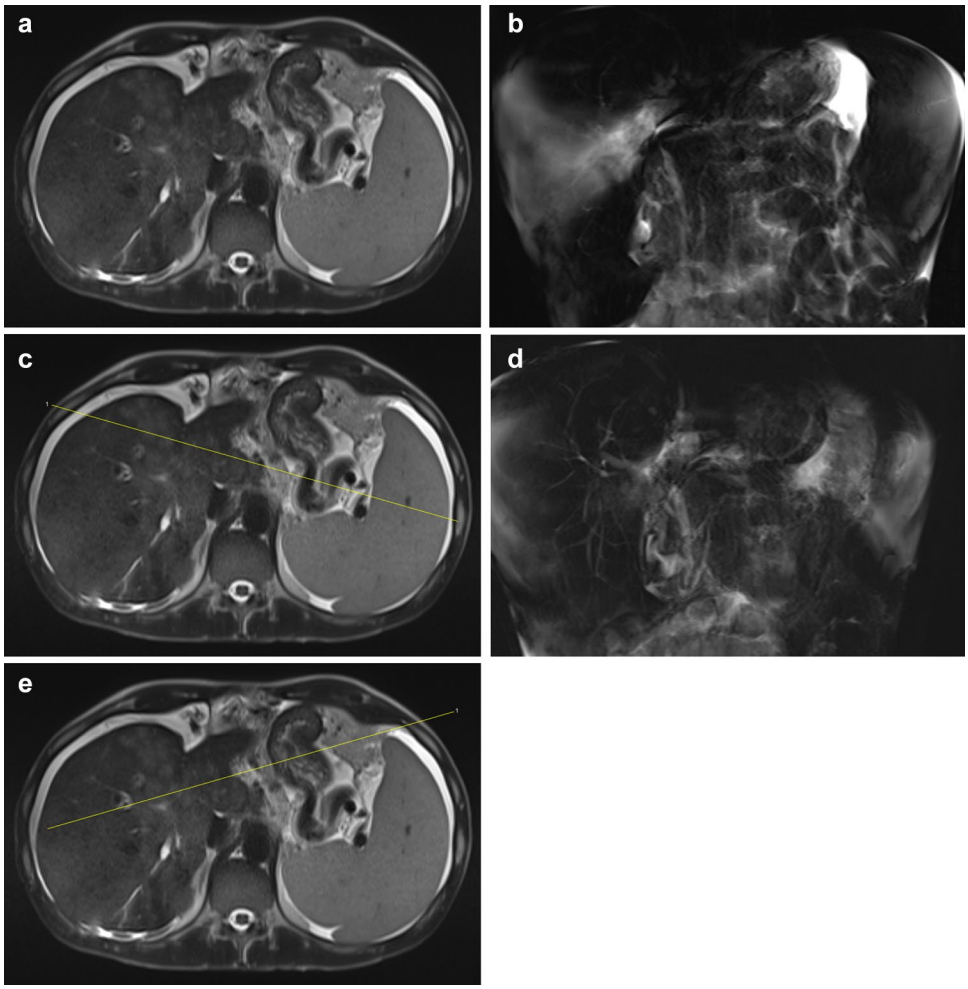

Fig. 17 MRCP findings obscured by ascites: 33-year-old male with cholangiocarcinoma undergoing MRCP for staging. (A) Axial T2-weighted images demonstrate moderate volume ascites. **B** Right oblique thick-slab MRCP (clockwise rotation from true coronal) along outlined plane in (**C**) with non-visualization of the right intrahepatic bile ducts right ducts due to being obscured by ascites. **D** Left oblique thick=slab MRCP (counter-clockwise rotation from true coronal) along outlined plane in (**E**) with well-visualized right intrahepatic bile ducts

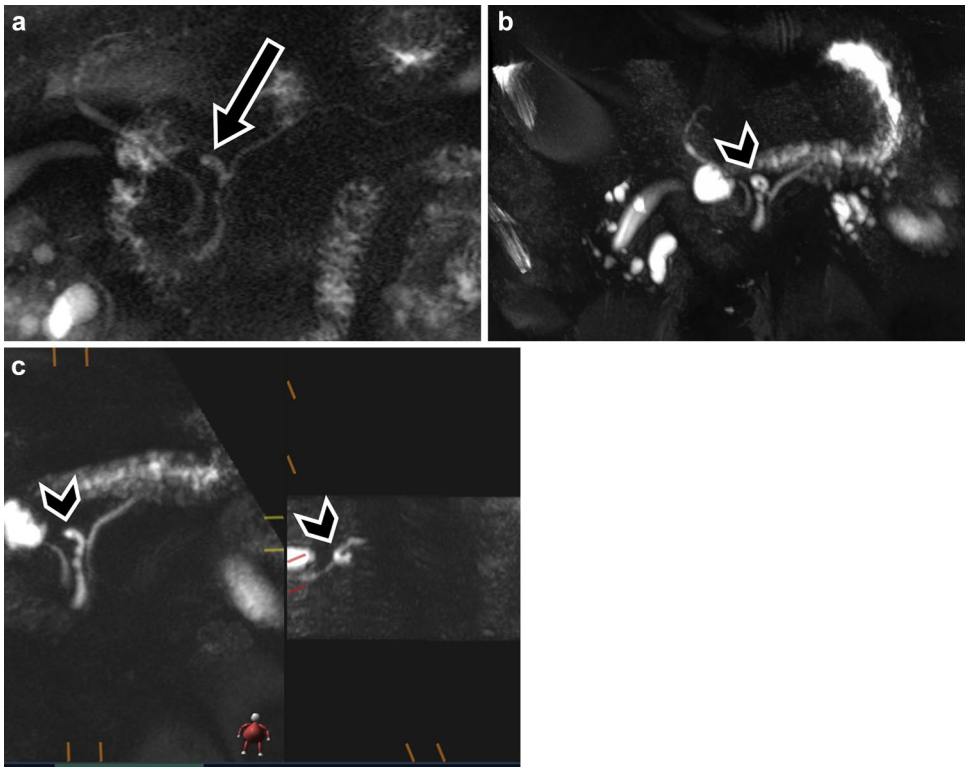

Fig. 18 Apparent lesion on MRCP due to pancreatic duct tortuosity: 67-year-old man undergoing MRCP for follow-up of a reported sidebranch intraductal papillary mucinous neoplasm. **A** 2D MRCP shows what appears to be a dilated sidebranch or a cystic lesion (arrow). **B** Rotating the MIP from the 3D MRCP and **C** curved reformats shows that the pancreatic duct makes a circuitous course, mimicking a dilated sidebranch. There were no pancreatic lesions

References

1. Dooms GC, Fisher MR, Higgins CB, Hricak H, Goldberg HI, Margulis AR (1986) MR imaging of the dilated biliary tract. Radiology 158 (2):337-341. doi:https://doi.org/10.1148/radiology.158.2.3941860
2. Wallner BK, Schumacher KA, Weidenmaier W, Friedrich JM (1991) Dilated biliary tract: evaluation with MR cholangiography with a T2-weighted contrast-enhanced fast sequence. Radiology 181 (3):805-808. doi:https://doi.org/10.1148/radiology.181.3.1947101
3. Kang SK, Heacock L, Doshi AM, Ream JR, Sun J, Babb JS (2017) Comparative performance of non-contrast MRI with HASTE vs. contrast-enhanced MRI/3D-MRCP for possible choledocholithiasis in hospitalized patients. Abdom Radiol (NY) 42 (6):1650–1658. doi:https://doi.org/10.1007/s00261-016-1039-6
4. Irie H, Honda H, Kuroiwa T, Yoshimitsu K, Aibe H, Shinozaki K, Masuda K (2001) Pitfalls in MR cholangiopancreatographic interpretation. Radiographics 21 (1):23-37. doi:https://doi.org/10.1148/radiographics.21.1.g01ja0523
5. Griffin N, Charles-Edwards G, Grant LA (2012) Magnetic resonance cholangiopancreatography: the ABC of MRCP. Insights Imaging 3 (1):11-21. doi:https://doi.org/10.1007/s13244-011-0129-9
6. Zhu L, Wu X, Sun Z, Jin Z, Weiland E, Raithel E, Qian T, Xue H (2018) Compressed-Sensing Accelerated 3-Dimensional Magnetic Resonance Cholangiopancreatography: Application in Suspected Pancreatic Diseases. Invest Radiol 53 (3):150-157. doi:https://doi.org/10.1097/RLI.0000000000000421
7. Zhu L, Xue H, Sun Z, Qian T, Weiland E, Kuehn B, Asbach P, Hamm B, Jin Z (2018) Modified breath-hold compressed-sensing 3D MR cholangiopancreatography with a small field-of-view and high resolution acquisition: Clinical feasibility in biliary and pancreatic disorders. J Magn Reson Imaging 48 (5):1389-1399. doi:https://doi.org/10.1002/jmri.26049
8. Merkle EM, Nelson RC (2006) Dual gradient-echo in-phase and opposed-phase hepatic MR imaging: a useful tool for evaluating more than fatty infiltration or fatty sparing. Radiographics 26 (5):1409-1418. doi:https://doi.org/10.1148/rg.265055711
9. Eason JB, Taylor AJ, Yu J (2013) MRI in the workup of biliary tract filling defects. J Magn Reson Imaging 37 (5):1020-1034. doi:https://doi.org/10.1002/jmri.23847
10. Li X, Liu Y, Ren K, Xu R, Xu K (2011) Findings of bile flow artifacts on MR cholangiopancreatography. Chinese Journal of Radiology 45 (9):850-853
11. Sugita R, Sugimura E, Itoh M, Ohisa T, Takahashi S, Fujita N (2003) Pseudolesion of the bile duct caused by flow effect: a diagnostic pitfall of MR cholangiopancreatography. AJR Am J Roentgenol 180 (2):467-471. doi:https://doi.org/10.2214/ajr.180.2.1800467
12. Morita S, Ueno E, Saito N, Suzuki K, Machida H, Fujimura M, Maruyama K, Onodera Y, Watanabe K, Suzuki T, Ohnishi T, Imura C, Mitsuhashi N (2008) Frequency of common bile duct motion artifacts caused by inferior vena cava pulsation on magnetic resonance cholangiopancreatography. Magn Reson Med Sci 7 (1):31-36. doi:https://doi.org/10.2463/mrms.7.31
13. Watanabe Y, Dohke M, Ishimori T, Amoh Y, Okumura A, Oda K, Hayashi T, Hiyama A, Dodo Y (2000) Pseudo-obstruction of the extrahepatic bile duct due to artifact from arterial pulsatile compression: a diagnostic pitfall of MR cholangiopancreatography. Radiology 214 (3):856-860. doi:https://doi.org/10.1148/radiology.214.3.r00mr09856
14. Phisalprapa P, Prachayakul V (2013) Ascariasis as an unexpected cause of acute pancreatitis with cholangitis: a rare case report from urban area. JOP 14 (1):88-91. doi:https://doi.org/10.6092/1590-8577/1257
15. Yu M, Huang B, Lin Y, Nie Y, Zhou Z, Liu S, Hou B (2019) Acute obstructive cholangitis due to fishbone in the common bile duct: a case report and review of the literature. BMC Gastroenterology 19 (1):177. doi:https://doi.org/10.1186/s12876-019-1088-8